Extrinsic or intrinsic conduction in cuprates: Anisotropy, weak, and strong links

J. Halbritter
Kernforschungszentrum Karlsruhe, IMF I, Postfach 3640, 76021 Karlsruhe, Germany
(Received 29 January 1993)

The layered structure of superconducting cuprates is the origin of the anisotropic conductivity in the normal state and the anisotropic energy gap and anisotropic critical current density j_c in the superconducting state. The anisotropic, quasi-two-dimensional conduction in the CuO_2 planes is close to the metal-insulator transition. Defects can either initiate insulating or conducting behavior depending on the position of the defects and orientation of the current. For example, defects may enhance the small conductivity $\sigma^{\perp}$ perpendicular to the planes, whereas defects reduce the strong conductivity $\sigma^{\parallel}$ along the planes. That is, defects make the cuprate superconductors more isotropic. Due to the layered structure defects are often organized in planes, usually of reduced conductivity, which are named "weak links" (WL). The effect of WL on the dc conductivity and superconductivity, especially as function of temperature and field, allows their classification and quantification. Their grain-boundary resistances $R_{bn}^{\parallel} \geq 10^{-7}$–$10^{-9}\ \Omega\,\mathrm{cm}^2$ are several orders of magnitude larger than the metallic Sharvin resistance, proving that WL are insulating interruptions. They contain localized states carrying current across by resonant tunneling. Such WL deteriorate the metallic conductivity $\sigma^{\parallel}$, the superconducting critical current $j_c^{\parallel}$, and the energy gap $\Delta_s^{\parallel}$, but enhance the leakage current $j_{bl}^{\parallel}$. Localized states between CuO_2 double planes enhance the "insulating" $\sigma^{\perp}$ and $j_c^{\perp}$ and deteriorate $\Delta_s^{\perp}$. For Y cuprates such states are due to oxygenation in the Cu chains. For Bi cuprates such states are caused by oxidation of the Bi oxide layers (overdoping). The intergranular $\sigma^{\perp}$ and $j_c^{\perp}$ in grain-aligned material are different for Y and Bi cuprates because Y cuprate surfaces decay above 70 K whereas the Bi-O surface stays stable up to 400 K containing even localized states. So $\sigma^{\perp}$ and $j_c^{\perp}$ are enhanced in grain-aligned Bi cuprates, which is the base of the brick-wall model. For all cuprates the $\sigma^{\parallel}$ and $j_c^{\parallel}$ degradation by WL is similar, due to the common two-dimensional nature.

I. INTRODUCTION

"Defects define properties of materials" or another crucial sentence "the knowledge of defects, i.e., of extrinsic properties, defines the intrinsic properties." These general sentences are particularly important for cuprates, especially for their electric conduction, because their intrinsic properties are not yet well known. Cuprates are layered compounds with (super) conduction confined to CuO_2 planes.[1,2] The quasi-two-dimensional conduction in narrow p-d bands is close to the metal-insulator transition[1–4] (MIT) so that most defects drive the cuprate insulating. Various studies on defects exist[5] but the relation, defective atomic arrangement and electric conduction, has not been drawn successfully. Or even worse: an ordered cation lattice at internal surfaces and degraded conduction seems no contradiction.[5] Also, evidence is presented that defects may enhance the small intrinsic perpendicular conductivity $\sigma^{\perp} \leq 1/\Omega\,\mathrm{cm}$, whereas the large intrinsic parallel conductivity $\sigma^{\parallel} \geq 10^4/\Omega\,\mathrm{cm}$ degrades by defects.

Because of this lack of knowledge it seems appropriate to use the normal conductivity and superconductivity itself to identify and classify defects. With this goal in mind, we first state that point defects in cuprates do not effectively scatter charge carriers. This is shown, e.g., by the long, temperature-dependent mean free paths $l(T \leq T_c) > 10$ nm.[6] In contrast, more effective in reducing the conductivity $\sigma^{\parallel}$ are planar, extended defects on μm scale occurring as external or internal surfaces perpendicular to the CuO_2 planes.[4,5] The so-called weak links (WL) show a locally degraded normal conductivity and superconductivity. The degradation of the normal conducting grain-boundary resistance $R_{bn}^{\parallel}$ ($\Omega\,\mathrm{cm}^2$) amounts to 2 to above 5 orders in magnitude hinting to a tunneling-type conduction mechanism. The conductivity degradation causes the current to meander on a μm scale through the cuprate network fundamentally affecting electrical transport in the normal and superconducting state in various ways.[7] The proposed, more intrinsic domain-wall interruptions on a nm scale[8] are not discussed here. This paper concentrates on WL on μm scale already identified, e.g., by conductivity degradation[4–7] or scanning-tunnel microscopy (STM).[9]

WL can be characterized by their ability to interrupt or to reduce the intrinsic normal or superconducting current along the ab direction. The atomistic model able to consistently describe all WL properties observed is summarized in Sec. II and Fig. 1 following Ref. 4: The two-dimensional p-d band with $n_s \geq 10^{21}/\mathrm{cm}^3$ as the carrier density is close to the metal-insulator transition in two dimensions occurring for $n_L < 10^{21}/\mathrm{cm}^3$, now, as density of localized states. At internal or external ab surfaces, dangling bonds have to rearrange and disorder, which may be enhanced by strain. This and the reduced overlap at surfaces renders the CuO_2 plane seams insulating containing plenty of localized states. Direct tunneling from the metallic banks and indirect tunneling via lo-

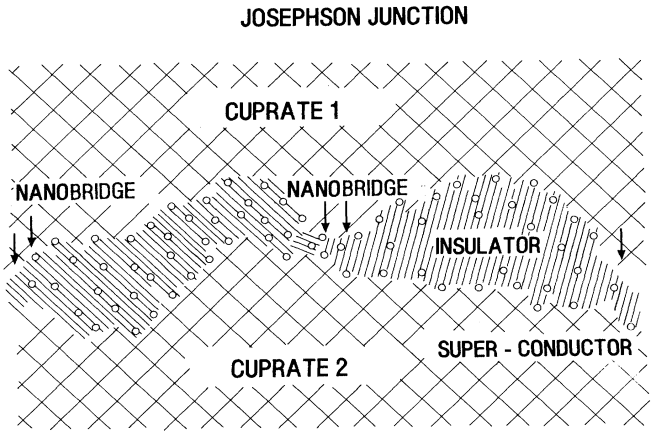

FIG. 1. Sketch of a small part of a planar intergrain (intra-) defect with localized states (O) in the insulator which mediate tunnel channels simulating nanoshorts. Such extended defects as small- or large-angle grain boundaries show up as weak links (WL) in conductivity measurements. At the banks of the cuprates the energy gap of localized states Δ_s is reduced reaching $\Delta_s \equiv 0$ in distances above 0.3 nm. $\Delta_s > 0$ yield a reduced critical current being reduced even more by the current carried via localized states in the middle of the barrier with $\Delta_s = 0$ as normal conducting, leakage current j_{bl} (Ref. 4). The "nanobridges" resemble optimal tunnel channels which may be the tip of "filaments" for deoxygenated or strained cuprate banks.

calized states carry the current across WL as quantitatively outlined in Sec. II A and compared with experiments in Sec. III A and for contact resistances in Sec. III B. Aside from tunneling across WL, tunneling is also the right word to describe conduction perpendicularly because of the confinement of p-d bonds to the CuO_2 planes with $\sigma^{\parallel} \geq 10^4/\Omega\,\mathrm{cm}$. The small intrinsic tunnel current $\sigma^{\perp} \leq 1/\Omega\,\mathrm{cm}$ is enhanced by localized states at the Fermi energy (E_F) and thus in cuprates the highest, intrinsic anisotropy occurs, usually in the most perfect crystals. The main known difference between Bi, Tl, and Y cuprates is found in this perpendicular conductivity $\sigma^{\perp}$: Whereas the Bi (Tl) cuprates cleave nicely between stable Bi (Tl) oxide planes, $YBa_2Cu_3O_{7-\delta}$ (YBCO) does not cleave well and the so obtained YBCO surfaces degrade easily and so does $\sigma^{\perp}$. In addition, by oxidation, localized states at E_F are created in the stable Bi oxide layer promoting resonant tunneling enhancing $\sigma^{\perp}$ and $j_c^{\perp}$ with a degraded gap $\Delta^{\perp}$. This is proposed as a reason for the applicability of the brick-wall model to grain-aligned Bi cuprates. In contrast, the degradation of Y cuprate surfaces shifts chain states away from E_F, degrading the intergranular $\sigma^{\perp}$ and $j_c^{\perp}$. Many properties of WL have been quantified experimentally by STM, break, or broad-area junctions.[4] Here in Secs. II B and III C the WL grain-boundary resistance is obtained also from the $\rho(T)$ analysis[7] combined with STM (Ref. 9). The normal conductivity is especially useful because there the charge carriers are measured dressed with different interactions, not being condensed in one superconducting $\rho \equiv 0$ state. As shown in Sec. III C, smaller $\rho^{\parallel}(0)$ and $d\rho^{\parallel}/dT$ values are indicators for higher quality samples.

In the superconducting state WL act as weak or strong Josephson junctions with properties given in Sec. II C. For *ab* WL depicted in Fig. 1, the Josephson critical current j_{cJ} is below values deduced from the grain-boundary resistance R_{bn} and the bulk superconduction energy gap Δ_0. The j_{cJ} degradation is accompanied by an increasing normal leakage j_{bl}. That intrinsic degradation is related to the quasi-two-dimensional conduction and so is the main source for the much reduced j_c values observed in cuprates compared to classical, three-dimensional superconductors. As outlined in Sec. II D, the j_{cJ} degradation and the leakage current j_{bl} are due to pair weakening at localized sites in a disordered environment and are strongest for *ab* surfaces. *c* surfaces are more inert and stay well ordered longer and so less degradation may occur in $j_c^{\perp}$ with smaller j_{bl}. As a consequence, a small $\sigma^{\perp}/\sigma^{\parallel}$ ratio may change in lowering the temperature through T_c yielding a current redistribution. But like for the ratio $\sigma^{\perp}/\sigma^{\parallel}$, the anisotropy of $j_c^{\perp}/j_c^{\parallel}$ becomes weaker by defects, see Sec. III D. In Sec. III E, consequences of WL on the superconducting critical current are outlined, e.g., being related to Josephson fluxon penetration at $H_{c1J} \ll H_{c1}$.[10,11] A method to identify and quantify WL is related to the leakage current given, e.g., by the surface residual resistance $R_J \propto j_{bl}$ and its field dependencies given by H_{c1J}. Because most knowledge is assembled for YBCO, in the following it is used as the model substance, if not stated otherwise.

II. MODELING OF CUPRATE INTERFACES

In this section the models elaborated in Ref. 4 and sketched in Fig. 1 are summarized and some crucial points and differences to classical metals are given.

First, being oxides, cuprate surfaces do not oxidize. Instead, they "relax the dangling bonds" yielding disorder on one hand but well bonded oxygen on the other hand. The instantaneous, intrinsic relaxation has to be contrasted to the natural oxidation of metals which is extrinsic in nature, takes time ($>$ min), and shifts defects out of the oxide (Fig. 2) yielding small values $n_L \leq 10^{18}/\mathrm{cm}^3$.

Second, the layered structure of cuprates with their highly directional p-d hybridization yields narrow, quasi-two-dimensional conduction bands with a small carrier density $n_s \geq 10^{21}/\mathrm{cm}^3$, only. Thus, in cuprates the density n_s is astonishingly close to the metal-insulator transition (MIT) observed[3] at $n_L \leq 10^{21}/\mathrm{cm}^3$ as density of localized states. This has to be contrasted to MIT in three dimensions for s electrons occurring slightly above $10^{18}/\mathrm{cm}^3$.

Third, relaxed *ab surfaces* render the cuprate insulating: by the reduced hybridization at surfaces especially in two dimensions, by the disorder related to relaxation or to strain. The relaxation corresponds to BaO formation[12] yielding hole reduction and localization in the CuO_2 planes found in x-ray photoelectron spectroscopy (XPS). The estimate of the localized hole density $n_L < 10^{21}/\mathrm{cm}^3$ fits to a hole distance of about 0.5–1 nm. The spatial MIT at interfaces with the ratio $n_s/n_L \approx 1$ has to be contrasted to classical metals with their oxide

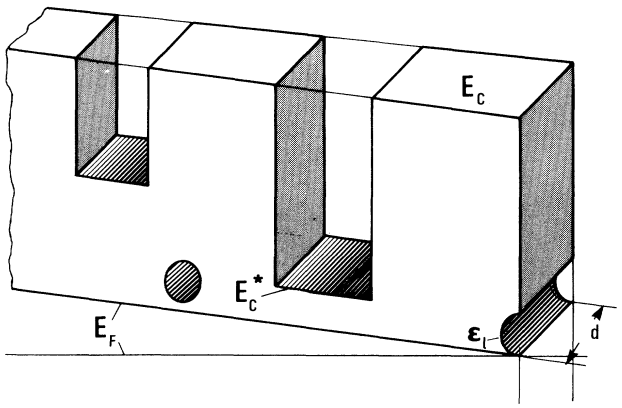

FIG. 2. Sketch of "real" tunnel barriers with $E_c(r)$ the lower edge of the conduction band. Until now, barriers $E_c(r)=E_c(x)$ being uniform along the electrodes have been treated, which cannot describe nanocrystalline or amorphous barriers, like Nb_2O_5 or perturbed YBCO. The model depicted corresponds to $(E_c-E_F)=\Phi\simeq 1$ eV for crystallites, $(E_c^*-E_F)=\Phi^*\simeq 0.1-0.2$ eV for channels, and $(E_F-\varepsilon_L)$ for resonant tunneling via localized states (n_L) symbolized as holes in the barrier. These three entities are the minimum set for the description of a barrier, where for YBCO $\Phi^*\geq 0.5$ eV and a white distribution of localized states for $|E_F-\varepsilon_L|<\Phi^*$ seems to hold. Estimates of n_L and the tunnel barrier heights are given in Table I.

coatings with $n_s/n_L>10^5$. As a consequence, the spatially sharp MIT of classical junctions (Table I) is in contrast to the smeared and roughened metal-insulator interface (MII) with an adjacent high $n_L\leq n_s$ in cuprate junctions and cuprate WL. The MII roughens further with higher temperatures T or voltages V and with smaller n_s, like a "surface roughening transition".[4,13] This "roughening" seems to connect to the filamentary fragmentation observed behind the WL, e.g., by deoxygenation.[14] As discussed in Secs. II A–II C, the high n_L densities yield strong indirect tunnel channels being pair weakened because of the disorder at such *ab* interfaces; see Fig. 1 and Sec. II C.

Fourth, c-axis surfaces obtained by cleavage or growth need less relaxation. For YBCO relaxation is stronger occurring already above 70 K (Ref. 15) in UHV. It seems to be related to BaO formation[12,16] because of the Ba plane or Cu chain forming the outermost layer. Angle-resolved XPS measurements[16,17] indicate that the relaxation extends down to the Y layer, leaving the upper half unit cell insulating. In contrast, Bi or Tl cuprates show inert BiO or TlO surfaces and thus they cleave nicely between the Bi (Tl) oxides planes[18] shielding, e.g., the crucial ^{12}Sr planes against relaxation. Hence the superconductivity of Bi or Tl cuprates stays intact up to the uppermost layer. In addition, by oxygenation, localized states at the Fermi energy E_F are induced[18] into the outermost oxide layer (overdoping). As a consequence $\sigma^\perp$ is large, e.g., in melt-textured Bi samples, and grows with oxygenation.

The atomistic interface considerations given in points 1–4 are modeled in Secs. II A–II C into tunnel channels and are compared with experiments in Sec. III. Before doing so, some general remarks are in order. Defects act differently in classical metals and in cuprates because of the adjacent MIT along the double CuO_2 planes and because of a small, insulating interlayer coupling perpendicularly. A consequence of the adjacent MIT is that the classical, elastic, point-defect scattering is negligible in CuO_2 planes. In contrast, resonant scattering or tunneling at localized states being organized to clusters is strong, mostly inelastic, and often pair weakening.[4] The most drastic example for clusters is the insulating seam at CuO_2 plane interfaces (WL), which reduce the conductivity by more than two orders of magnitude (Sec. II A). Thus, a conductivity description of WL is no longer adequate and in the following is substituted by the "interface resistance $R_{bn}\geq 10^{-9}\ \Omega\,\mathrm{cm}^2$." The tunneling in the perpendicular direction has an intrinsic resistance[4] $R^\perp\geq 10^{-4}\ \Omega\,\mathrm{cm}^2$ for the Bi cuprate. This value is reduced by defects allowing resonant tunneling in parallel. Thus, defects enhance $\sigma^\perp$ and reduce $\sigma^\parallel$ making cuprates more isotropic. In the superconducting state, aside from the conductivities the bulk energy gap $\Delta_0\approx 20$ meV and the surface states gap $\Delta_s<\Delta_0$ are important for the superconducting Josephson current $j_{cJ}\propto\Delta_s$ and for the normal conducting leakage current j_{bl}, see Fig. 1 and Table I.

For *ab* interfaces depicted in Fig. 1, in CuO_2 planes the first row of oxygen $\delta x\approx 0.2$ nm in front of the supercon-

TABLE I. Density of metallic (n_s) and localized (n_L) states in some typical junctions. Here n_L is an upper limit for Nb-Nb_2O_5 naturally growing in air (Ref. 20), whereas n_L of cuprate junctions is related to intrinsic degradation. As consequences of localized states, pair weakening and new, parallel channels show up. These new channels do not participate in the Josephson critical current j_{cJ} but contribute to the normal leakage current $j_{bl}\propto 1/R_{bl}$.

Metallic banks	E_F (eV)	n_s (cm^3 eV)	Barrier	Φ (eV)	n_L (cm^3 eV)	d (nm)	I_cR_{bn} (units of $\pi\Delta/2e$)	R_{bn} (units of R_{bl})
Nb	6	$>10^{22}$	Nb_2O_5	0.1 1	$\leq 10^{17}$	$\simeq 2$	≤ 0.9	<0.1
YBCO	≤ 0.3	$\geq 10^{21}$	YBCO$^{*\parallel}$	$\simeq 1$	$\leq 10^{21}$	$\simeq 2$	<0.6	$>0.1-0.9$
BSCCO	≤ 0.3	$\geq 10^{21}$	BSCCO$^{*\parallel}$	$\simeq 1$	$\leq 10^{21}$	$\simeq 2$	<0.6	$>0.05-0.9$
YBCO	≤ 0.3	$\geq 10^{21}$	YBCO$^{*\perp}$	$\simeq 1$	O-DEP	0.8	≤ 1	≤ 0.1
BSCCO	≤ 0.3	$\geq 10^{21}$	BSCCO$^{*\perp}$	$\simeq 1$	O-DEP	1.2	≤ 1	≤ 0.1

ductor has a well-defined overlap to the adjacent superconducting sites. $\Delta_s \approx 0.4\Delta_0 \simeq 8$ meV has been estimated for such surface states. For larger distances $\Delta_s(\delta x)=0$ holds, causing resonant tunneling to become the normal conducting, leakage tunnel current j_{bl} (Sec. II C).

A. Tunnel channels across cuprate interfaces

Starting with the intrinsic, two-dimensional conduction along the CuO_2 planes in YBCO of $\sigma^{\parallel}(100\ \mathrm{K}) = 2\times10^4/\Omega\,\mathrm{cm}$ and $l \simeq 5\times10^{-7}$cm as mean free path,[6] the Sharvin resistance[19] is given by

$$R^{\parallel}_{\mathrm{sh}} \simeq 2l/\sigma^{\parallel} \simeq 5\times10^{-11}\ \Omega\,\mathrm{cm}^2\ . \tag{2.1}$$

R_{sh} is the intrinsic grain-boundary resistance of "clean interfaces." Due to the insulating seam (Fig. 1) with its localized states n_L, the current across WL is a tunnel current. Using d as the barrier width and $\Phi \simeq 1$ eV as the barrier height, the wave functions decay away from the metallic banks like $\exp(-\kappa_0\delta x)$ with $\kappa_0 \simeq 7/\mathrm{nm}$ yielding with n_s as the carrier density in the banks (Fig. 2),[4]

$$R^{\parallel}_{bn} \approx 10^{-9}\ \Omega\,\mathrm{cm}^2 \ \text{ for } d \simeq 1\text{–}1.5 \text{ nm, and } n_L \approx 10^{20}/\mathrm{cm}^3$$

and (2.2)

$$R^{\parallel}_{bn} \approx 10^{-7}\ \Omega\,\mathrm{cm}^2 \ \text{ for } d \simeq 2.5\text{–}3 \text{ nm,}$$

$$\text{and } n_L \approx 10^{20}/\mathrm{cm}^3\ .$$

Aside from the elastic tunnel channels[20] j_D ("direct") and j_R ("resonant") inelastic, multihop channels j_I exist increasing strongly with temperature T and voltage U. This may be the cause for most $I(U)$ characteristics observed.[4] For strained and deoxygenated YBCO tunnel channels seem the tip of a high conductivity filament connecting WL with the bulk metal in 1–100 nm depth. This filamentary branching seems related to O disorder or O loss as observed by optical or small spot electron-energy-loss spectroscopy measurements.[14,21]

In c direction the p-d amplitude of the CuO_2 planes is small and thus the transport $\sigma^{\perp}$ can be said to be due to tunneling. Taking the above values $\Phi \simeq 1$ eV as tunnel barrier $R^{\perp} \propto \exp(2\kappa_0 d)$ yields[4]

$$R^{\perp} \simeq 10^{-4}\ \Omega\,\mathrm{cm}^2$$

$$\text{for 2:2:1:2 compounds with } d = 1.2 \text{ nm}\ , \tag{2.3}$$

yielding

$$R^{\perp} \simeq 3\times10^{-6}\ \Omega\ \mathrm{cm}^2 \ \text{ for YBCO with } d \simeq 0.8 \text{ nm}\ , \tag{2.4}$$

corresponding to $\rho^{\perp} \approx 10\text{–}100\ \Omega\,\mathrm{cm}$. Any localized state between the CuO_2 planes at E_F (Ref. 4) yield a resonant tunnel current $j^{\perp}_R$ in parallel, which short circuits the large intrinsic resistance $R^{\perp}$ of Eq. (2.4). Contact resistances in $\parallel$ or $\perp$ direction are given by Eqs. (2.1)–(2.4) also—see Sec. III B.

B. Resistance and percolation by weak links

The grain-boundary resistances $R^{\parallel}_{bn} \propto \exp(\kappa_0 d)$ of WL introduced in Eq. (2.2) are effectively insulating for barriers width $d \geq 5$ nm forcing the current to meander through the material to avoid those WL as sketched in Fig. 3. For the resistivity this and better conducting WL yield a kind of effective medium ansatz:[7]

$$\rho(T) = R^J_{bn}/a_J + p\,(\alpha^i T + \rho^i_{0L} + R^G_{bn}/a_G)\ , \tag{2.5}$$

with[22] $\alpha^i \simeq 0.5\ \mu\Omega\,\mathrm{cm/K}$ and $\rho^i_{0L} \simeq -40\ \mu\Omega\,\mathrm{cm}$ as intrinsic values for fully oxygenated YBCO. Here ρ^i_{0L} is defined by linear extrapolation around $T \approx 300$ K and $a_{J/G}$ is the mean distance between WL. The geometrical factor $p > 1$ accounts for the mean percolative lengthening of the conduction path and shrinking of the current cross sections[7] sketched in Fig. 3. Equation (2.5) is an extension of Eq. (1) in Ref. 7 taking into account differences between intergrain—R_J and a_J—and intragrain boundaries—R_G and a_G. R_J and a_J describe well accepted "grain" properties, e.g., of sintered cuprates. Subgrain boundaries with R_G in mean distances a_G became obvious experimentally recently by STM,[9] showing islands in epitaxial growth. "Subgrain boundaries" are small- or large-angle grain boundaries, where epitaxially growing islands fuse together. In Sec. III C, R_G and R_J are evaluated and compared with $R^{\parallel}_{bn}$ [Eqs. (2.1)–(2.4)] using experimental obtained $\rho(0)$ and p values. The method of deducing R_{bn} by normal conducting measurements is superior to the use of the superconducting critical current j_c. This is due to the fact that only the normal state allows a quantitative estimate of R_{bn} and a_i or ρ^i_{0L} by Eq. (2.5) by their finite and different resistances. In the superconducting state $\rho \equiv 0$ holds, in contrast, making quantification difficult, as discussed in Sec. III E.

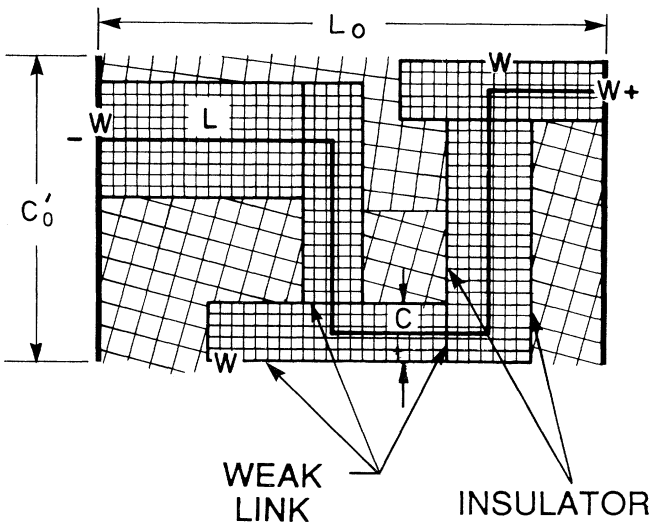

FIG. 3. Sketch of a unit for current path lengthening ($L/L_0 > 1$) and cross section shrinking ($C/C_0 < 1$) by planar defects in cuprates. These units may be interconnected in parallel and in series via weak links.

C. WL leakage current and superconducting critical current

Historically, weak links became obvious by the very much deteriorated critical currents $j_c < 10^3$ A/cm^2 in sin-

TABLE II. Parameters characterizing weak links and bulk, intrinsic YBCO at $T=0$ assembled in Refs. 4, 7, 11, and 19 from experiments. The abbreviations "*J*" or "*G*" or "*I*" are subscripts added as needed for clarity. The critical currents $j_{cJ/G}$ cited are Josephson critical currents, which together with pinning yield the actual measured critical current j_c sketched in Fig. 4. The fluxoids entering at H_{c1J} are Josephson fluxons for intergrain weak links turning to a more Abrikosov-like fluxon for the "*G*" and "*I*" system. Josephson fluxons move as linear array only, which yields large activation energies $U(T)$ proportional to the length of the weak links for fluxon motion.

Weak link	Abbr.	R_{bn} (Ω cm^2)	j_c (A/cm^2)	λ_J (μm)	H_{c1} (Oe)	U (eV)
Insulator		∞	0	∞		
Intergrain	*J*	$\geq 10^{-7}$	$\sim 10^2$	~ 30	~ 1	$\sim 1-10$
Intragrain	*G*	$\geq 10^{-9}$	$\geq 10^4-10^7$	~ 1	~ 100	$\sim 0.01-1$
Intrinsic	*I*	0	$\geq 10^9$	0.14	≥ 1000	?

tered cuprates degrading further at small fields $H \leq 10$ Oe. Small Josephson critical currents j_{cJ} are a manifestation of large WL resistances R_{bn} discussed in Sec. II A. The mean Josephson critical current is obtained by averaging over individual tunnel channels in the WL area A:

$$j_{cJ}=\sum_i I_c^i/A\,;\quad R_{bn}=1/\sum_i 1/R_{bn}^i\ , \tag{2.6}$$

where

$$\sum_i j_{cJ}^i R_{bn}^i=\sum_i \frac{\pi\Delta^i(T)}{2e}\tanh\frac{\Delta^i(T)}{2kT} \tag{2.7}$$

holds. The individual energy gaps Δ^i of localized sites are smaller than the bulk energy gap $\Delta_0\approx 20$ meV due to Coulomb repulsion by the "localization of a Cooper pair."[4] For the first layer of localization in 0.2 nm distance to the cuprate $\Delta^i\simeq 0.4\Delta_0\simeq 8$ meV holds. For the next layer (≥ 0.4 nm) the energy gap $\Delta^i\approx 0$ is negligible and so is the Cooper pair current $j_{cJ}^i\simeq 0$. Such states give rise to the normal conducting leakage current $j_{bl}\propto\exp(-\kappa_0 d)$ by resonant tunneling. According to Sec. II A, WL with $d>0.5$ nm show[4]

$$j_{cJ}R_{bn}\propto\frac{\bar{n}_s\exp(-2\kappa_0 d)}{\bar{n}_s\bar{n}_L\exp(-\kappa_0 d)}\propto\frac{1}{\bar{n}_s\bar{n}_L^2 R_{bn}(d)}\ , \tag{2.8}$$

by the dominant resonant tunneling in the normal state $R_{bn}\propto\exp(\kappa_0 d)$ and "direct" Cooper pair tunneling $j_{cJ}\propto\exp(-2\kappa_0 d)$. The exponential dependences give larger weight to small distances d^i and large n_L^i values. As shown in Fig. 1, optimal localized states cause a spatially confined tunnel channel of 1 nm size with a j_{c0} approaching the bulk limit of about 5×10^8 A/cm^2. Such nanochannels carry supercurrent in fields above 5 T and are found in bicrystal[23] junctions and bulk cuprate superconductors.[24] An alternative explanation of Eq. (2.8) is given by Moeckly, Lathrop, and Buhrman[14] by filamentary fragmentation by deoxygenation or strain.

As a form of the Meissner effect, Josephson junctions expel magnetic field with[10]

$$\lambda_J=\sqrt{\hbar/2\mu_0 j_{cJ}(T,H)e\lambda_I(T)}\ , \tag{2.9}$$

as the Josephson penetration depth which is usually much larger than the intrinsic penetration depth λ_I see Table II. For fields above

$$H_{C1J}\simeq\phi_0/4\pi\lambda_I\lambda_J\simeq H_{C1}\lambda_I/\lambda_J\ , \tag{2.10}$$

Josephson fluxons penetrate into WL where $j_{cJ}(H)$ degrades by interference effects. The $j_{cJ}(H)$ degradation is sketched in Fig. 4 for the different types of WL. For fluxon distances comparable to distances between "nanobridge irregularities" of WL (see Fig. 1), $j_{cJ}(H)$ becomes H-field independent shown in Fig. 4. This case has recently been simulated by pinning of Josephson fluxons.[25] The plateau may be identified with H_{C2J} fields introduced in earlier papers of the author.[11] But as stated in Ref. 25, j_{cJ} stays finite till $H_{c2}\approx 100$ T of the bulk is reached.

The above j_{cJ} reductions [Eqs. (2.6)–(2.9)] are compensated by an enhanced normal leakage current $j_{bl}\propto 1/R_{bl}\propto 1/R_{bn}$ via the normal ($\Delta^i=0$) intermediate

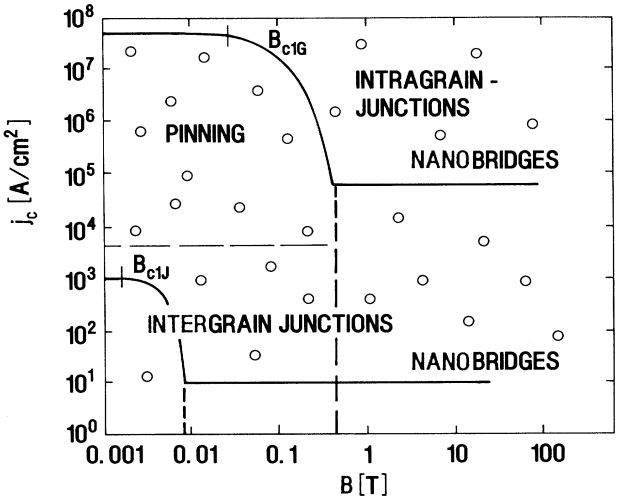

FIG. 4. Typical j_c ($T<10$ K, H) dependencies obtained for polycrystalline and "single crystalline" $YBa_2Cu_3O_7$. Pinning is symbolized by "O" where the distribution of O in this sketch has no significance to a "pinning force". Above the fluxon penetration field $H_{c1J/G}$ the Josephson fluxons dephase both banks of the WL reducing critical currents $j_{cJ/G}(H)$. For fluxon distances matching to nanobridge distances $j_{cJ/G}$ becomes nearly field independent. Depending on preparation the indicated absolute values may vary by orders of magnitude.

states. $j_{bl}(T,H)$ is measured in tunneling at small bias but most dramatic is the consequence on rf residual losses[11]

$$R_J=(\omega\mu_0)^2\lambda_J^3 2a/R_{bl} \ . \tag{2.11}$$

For || WL the direct, Josephson tunneling is separated from resonant, normal tunneling. But as proposed in Ref. 4, indirect Cooper pair tunneling may exist for cases, where the intermediate states belong to an ordered environment. These extended intermediate plaques carry Cooper pairs in $PrBa_2Cu_3O_7$ and in $j^{\perp}$ via states at E_F. Seemingly, the ordered environment allows the Cooper pair to smear out enough avoiding pair weakening via Coulomb repulsion.[4]

III. COMPARISON WITH EXPERIMENTS

Intrinsic properties are not known *a priori* and so extrinsic properties have to be identified first. Extrinsic is usually understood to be a consequence of defects. Defects used in this paper are localized states and WL. Introduced in Sec. II are consequences of the defects as reduced metallic conduction parallel (||) to the CuO_2 planes and a reduced energy gap $\Delta_s<\Delta_0$. In summary, "intrinsic" is proposed to be related to the largest $\sigma^{\parallel}$ and $\Delta_0^{\parallel}$. In the insulating, perpendicular ($\perp$) direction, intrinsic is proposed to be related to the highest resistances $\rho^{\perp}$ and largest gap values $\Delta_0^{\perp}$. Experiments are analyzed in the following using these guidelines.

A. Interface resistances $R_{bn}^{\parallel}$ and $R^{\perp}$

Artificial and natural tunnel junctions are analyzed in Ref. 4 and related to different tunnel channels. Here natural WL are analyzed phenomenologically. The most elaborate analysis was done by Russek and co-workers[26] by singling out one WL in epitaxial films on MgO. They found an increase of $R_{bn}^{\parallel}\simeq 10^{-9}\ \Omega\,\mathrm{cm}^2$ to $\simeq 10^{-7}\ \Omega\,\mathrm{cm}^2$ by deoxygenation following

$$j_{cJ}R_{bn}\propto 1/R_{bn} \ . \tag{3.1}$$

In fully oxygenated WL, $R_{bn}^{\parallel}$ is about a factor 100 larger than the intrinsic Sharvin resistance R_{sh} [Eq. (2.1)]. This factor 100 and the reduction of $j_{cJ}R_{bn}\propto l/R_{bn}$ confirms the model presented in Sec. II C where localized states resonantly carry the normal current [Eq. (2.8)] with $n_L\simeq 10^{20}/\mathrm{cm}^3$ independent of barrier width d.

The large increase by a factor of 100 in Eq. (3.1) fits the exponential dependence of $R_{bn}\propto\exp(+\kappa_0 d)$ on d. The growth of d from 1 to 2 nm with deoxygenation is explained by the $\rho(100\ \mathrm{K})$ or $d\rho/dT$ increase by factor of 2,[27] corresponding to a decrease of n_s by a factor of 2. The n_s decrease smears out the MII and effectively retracts this interface resulting in the d increase.[4] According to Moeckly, Lathrop, and Buhrman[14] the MII together with its surface roughening[13] connects to a filamentary fragmentation of the metal growing with deoxygenation and strain. Worthwhile to mention is the decrease of j_{cJ} by four orders of magnitude as compared to the R_{bn} increase by two orders. This large j_{cJ} decrease is not due to a degraded surface energy gap Δ_s but due to parallel tunnel channels feeding j_{bl}. The naturally grown WL as small- or large-angle grain boundaries are inhomogeneous on an atomic scale, as found by STM (Ref. 9) or $j_{cJ}(H)$ (Refs. 21, 23–26). In my model, this is a consequence of resonant tunneling via localized states of a relaxed interface as depicted in Fig. 1. $j_{cJ}(H)$ is explained well assuming the effective diameter of a tunnel channel with 1 nm being 5 nm apart[23] for small-angle boundaries. The "1-nm channels" may have locally $R_{bn}^{*}\approx 10^{-10}\ \Omega\,\mathrm{cm}^2$, which is still above the Sharvin resistance but below observed values $R_{bn}\sim 10^{-9}\ \Omega\,\mathrm{cm}^2$ [Eq. (3.1)].[26] By deoxygenation these microshorts—or better, nanoshorts—like the more insulating WL rest, are filamentarily separated from the bulk because of the bulk-O loss from the chains,[14] in line with Eq. (3.1). As in the bulk,[27] also at the interface, O

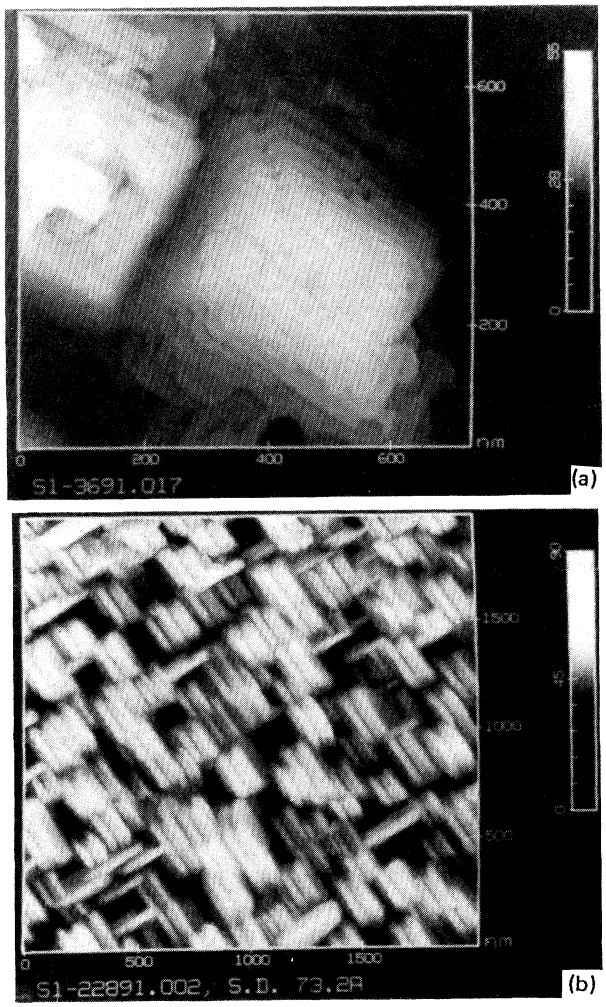

FIG. 5. Typical STM image of $YBa_2Cu_3O_7$ 200-nm thick deposited on MgO (100) single-crystal substrates at standard deposition conditions. (a) c-axis films with grains of about 0.5–1 μm. (b) a-axis films with grains of about 0.2 μm length (Hawley *et al.*, Ref. 9).

loss or O ordering plays a crucial role in defining the nanoshorts[14] and so j_{cJ} and j_{bl}. Different densities of nanoshorts with $R^{*}_{bn} \approx 10^{-10}$ $\Omega\,\mathrm{cm}^2$ are proposed as the "atomistic base" of small- or large-angle grain boundaries of well oxygenated and well relaxed YBCO.[5] Such subgrain boundaries are called intragrain WL, see, e.g., Fig. 5. In sintered material the contact area shrinks and other WL types (Fig. 6) occur in random orientation yielding $R_{bn} \simeq 10^{-7}$–10^{-5} $\Omega\,\mathrm{cm}^2$ on average. But still some "microshorts" exists shown in the high-field j_{cJ} data sketched in Fig. 4. Their density can be enhanced by proper aligning.[24]

Other types of WL are nucleated at artificial substrate defects individually[28,29] or by growth conditions as in the case of *a*-axis films (Ref. 30) or specific 305 $SrTiO_3$ (Ref. 31) or 101 $SrTiO_3$ and $LaAlO_3$ (Ref. 30) substrates. The best studied bicrystal WL on $SrTiO_3$ show[28]

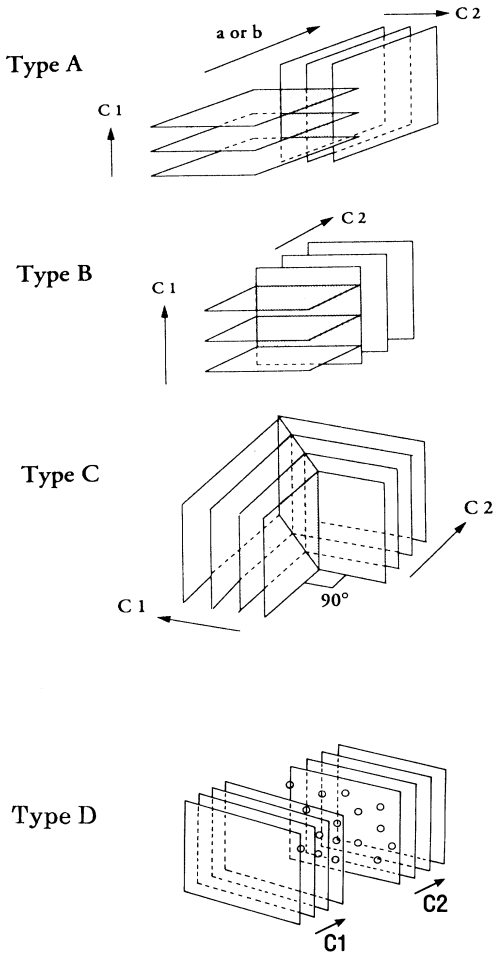

FIG. 6. Schematic diagrams of various grain boundaries; a 90° [010] twist boundary (type *A*), a 90° [010] basal-plane-faced tilt boundary (type *B*), a 90° [010] symmetrical tilt boundary (type *C*) and a boundary joining parallel CuO_2 planes (type *D*). In types *A*–*D* the current is carried by localized states sketched in Fig. 1. In type *D* the sketched localized states belong to the Cu chains (YBCO) or Bi oxides (Tl oxide) layers in Bi (Tl) cuprates.

$$R_{bn} \geq 10^{-8}\ \Omega\,\mathrm{cm}^2; \qquad j_{cJ} R(\Theta)_{bn} \propto 1/R(\Theta)^{m}_{bn} \ \text{ with } m \simeq 1.2\ . \tag{3.1'}$$

The exponent $m = 1.2$ for bicrystals WL differing from $m = 1$ for WL changing by deoxygenation[26] can be related to the dependence of n_L on width d or filaments.[14] d or $1/n_L$ or the density of "nanoshorts" or filaments changes with bicrystal orientation angle Θ. But it should be mentioned that $R_{bn} \geq 10^{-8}$ $\Omega\,\mathrm{cm}^2$ of bicrystal WL is large to start with. With optimal growth conditions $R_{bn} \simeq 10^{-9}$ $\Omega\,\mathrm{cm}^2$ have been achieved for artificial WL of type *C* (Fig. 6),[29] also.

The tunnel current perpendicular to the CuO_2 planes is small with intrinsic $R^{\perp}$ values between adjacent CuO_2 double planes of 10^{-4} $\Omega\,\mathrm{cm}^2$ (2:2:1:2) or 3×10^{-6} $\Omega\,\mathrm{cm}^2$ (YBCO). Defects, e.g., by oxygenation, strengthen tunneling and reduce $R^{\perp}$ and $\rho^{\perp}$. For example, for 2:2:1:2 a reduction from 40 to about 1 Ω cm has been observed by overdoping,[32] whereas for YBCO oxygenation from $O_{6.8}$ to about $O_{6.9}$ reduced $\rho^{\perp}$ from 100 to about 2 m Ω cm.[33] At external YBCO surfaces the conductivity degrades intrinsically by relaxation,[15,17] enhancing $R^{\perp}$ of such surfaces. This does not happen, usually, for Bi and Tl cuprates, where by oxygenation (overdoping) localized states at E_F are generated[18] reducing $R^{\perp}$ in addition. Thus, intergranular $R^{\perp}$ of YBCO are above 3×10^{-6} $\Omega\,\mathrm{cm}^2$, but for 2:2:1:2 $R^{\perp}$ and $\rho^{\perp}$ decreases from 40 Ω cm to about 1 Ω cm and $\Delta^{\perp}$ from 20 meV to less than 1 meV.[32] This yields

$$j_c^{\perp} R^{\perp} \propto 1/(R^{\perp})^{m}, \quad m < 0.5\ , \tag{3.2}$$

such as in the case of PBCO junctions.[4] Thus the "ordered states at E_F in BiO" seem extended as to allow Cooper pair tunneling via those weakly superconducting plaques. The existence of "plaques" is also obvious from the $a^{\perp}$ estimates in Sec. III C. Another consequence of the plaques is a small amount of leakage current $j_{bl}^{\perp}$ as evidenced by STM, broad-area, and break-junction results.[28]

B. Contact resistances

Metal-cuprate contacts have been studied for the current transfer parallel (||) and perpendicular ($\perp$) to the CuO_2 planes.[35,36] With contact to Pb or Ag in the || case,

$$R_c^{\parallel} \geq 10^{-9}\ \Omega\ \mathrm{cm}^3 \tag{3.3}$$

is observed fitting in all properties to the internal degradation of YBCO described in Eq. (2.2). Thus, also in this case the YBCO surface is relaxed to an insulator with localized states and the higher density of states in Pb or Ag does not enhance $R_c^{\parallel}$ markedly over $R_{bn}^{\parallel}$ of Eq. (2.2). For $\perp$ contacts Eq. (2.4) is the starting point with $R^{\perp} \simeq 3\times10^{-6}$ $\Omega\,\mathrm{cm}^2$ for YBCO. For YBCO the degraded upper half cell of about 0.8-nm thickness and the higher density of states in, e.g., Ag with *s*-electron-type overlap reduces $R^{\perp}$ to

$$R_c^{\perp} \geq 10^{-8}\ \Omega\,\mathrm{cm}^2\ . \tag{3.3'}$$

This is in agreement with contact resistances to epitax-

ial films.[36] Often Ag overlayers are annealed (>200 °C) causing diffusion of Ag into weak links enhancing the surface area and making use of the smaller value $R_c^{\parallel} \approx 10^{-9}\ \Omega\,\mathrm{cm}^2$.

C. $\rho(T)$ analysis and weak-link resistivities R_{bn}

In Sec. II B the analysis of $\rho(T)$ was outlined to deduce the WL resistances R_{bn}. Epitaxial films or single crystals have by definition no intergrain boundaries, i.e., $R_J \equiv 0$ and thus Eq. (2.5) writes[7,30]

$$R_{bn}^G / a_G \leq 10\ \mu\Omega\,\mathrm{cm}, \quad R_{bn}^G \geq 10^{-9}\ \Omega\,\mathrm{cm}^2\ , \tag{3.4}$$

with $a_G \leq 1\ \mu$m for such epitaxial c-axis films (Fig. 5). Epitaxial a-axis films (Fig. 5) show $p \geq 2$, $\rho(0) \geq 0.6$ mΩ cm, and $a_G \approx 0.2\ \mu$m,[30] yielding

$$R_{bn}^G \geq 5 \times 10^{-9}\ \Omega\,\mathrm{cm}^2\ . \tag{3.5}$$

Hence, a- and c-axis films have the same type of weak links R_{bn} wise, despite the different boundary angle Θ. For c-axis films Θ is small and large for a-axis films with $\Theta = 90°$. This is in line with a recent finding that natural WL, if properly prepared, carry the same current for $0 \leq \Theta \leq 90°$.[37] In Ref. 30 several types of WL have been proposed depicted in Fig. 6. The above finding indicates that type C has the smallest resistance R_{bn}^G and the current will pass through such WL as to minimize $\rho(T)$. Experimental estimates of the other WL types are difficult because the lack of well-defined type A or B samples. Polycrystalline, randomly oriented YBCO has typically[7] $\rho(0) \geq 10^{-4}\ \Omega\,\mathrm{cm}$ and grain sizes $a_J \geq 10^{-3}$ cm yielding

$$R_{bn}^J \geq 10^{-7}\ \Omega\,\mathrm{cm}^2 \quad \text{and } p \geq 3 \tag{3.6}$$

because of the random orientation of grains. It seems likely that these large intergrain resistances are due to a small density of nanoshorts by the lack of alignment, i.e., the WL are of type A or B (Fig. 6), or other random orientations. By proper alignment[24] higher $j_{cJ}(H > 0.1$ T) are measured showing the preference of type C. In extended, polycrystalline material, parallel shunting of grains by intergrain weak links reduce $\rho(0)$ but enhance p.[30] This tendency has been found for 103 epitaxial films also.

Taking the metalliclike conduction in the c direction in single crystals[32,38,39] or epitaxial film[31] Eq. (2.5) results in

$$\begin{aligned} &p^{\perp} > 30-1000, \quad \rho^{\perp}(0) \geq 0.002-10\ \Omega\,\mathrm{cm}, \\ &\text{and } R_{bn}^{\perp} \geq 10^{-8}\ \Omega\ \mathrm{cm}^2 \end{aligned} \tag{3.7}$$

using $a^{\perp} \simeq 1\ \mathrm{nm} \times p^{\perp} \simeq 30-1000$ nm describing the zig-zag conduction. For $\rho^{\perp} > 6$ mΩ cm activated conduction shows up, in line with a minimum Mott-Anderson metallic conductivity[3c] for the coupling of planes. $p^{\perp}$ depends only slightly on preparation, whereas $\rho^{\perp}(0)$ increases drastically with deoxygenation because then states at E_F from the Cu chains and BiO are lost. The intrinsic

$$\begin{aligned} \rho_i^{\perp}(0) = R_{bn}^{\perp} / a_i^{\perp} &= 10^{-4}\ \Omega\,\mathrm{cm}^2 / 1.2 \times 10^{-7}\ \mathrm{cm} \\ &\simeq 10^3\ \Omega\,\mathrm{cm}\ (2{:}2{:}1{:}2) \end{aligned}$$

or

$$\begin{aligned} \rho_i^{\perp}(0) &= 3 \times 10^{-6}\ \Omega\,\mathrm{cm}^2 / 0.8 \times 10^{-7}\ \mathrm{cm} \\ &= 40\ \Omega\,\mathrm{cm}\ (\mathrm{YBCO}) \end{aligned}$$

is well above measured values. Hence, several "barriers" are shunted by localized states, already. This together with the observation of Ref. 32 that with $\rho^{\perp}$ reduction $\Delta^{\perp}$ decreases in parallel confirms our model,[4] that $p^{\perp}(T)$ and $\rho^{\perp}(T)$ [Eq. (3.7)] are mainly due to weak links connecting the highly conducting CuO_2 planes by defects. That is, the large $p^{\perp}$ in Eq. (3.7) is due to zig-zag conduction through the crystal using high conductivity $\sigma^{\parallel}$ paths and perpendicular, resonant tunnel paths in distances $a^{\perp} > 30$ nm. By pair weakening[4] the localized states have a lowered energy gap and by resonant tunneling the defects reduce $\rho^{\perp}$ drastically. In this connection for YBCO the intrinsic $R^{\perp} \simeq 3 \times 10^{-6}\ \Omega\,\mathrm{cm}^2$ should be mentioned yielding as intrinsic anisotropy $R^{\perp}/R_{\mathrm{sh}}^{\parallel} \approx 5 \times 10^5$. This high anisotropy is reduced by defects, which by their low resistance $R^{\perp} \sim 10^{-8}\ \Omega\,\mathrm{cm}^2$ [Eq. (3.7)], shunt the CuO_2 planes and by $R_{bn}^{\parallel} \simeq 10^{-7}-10^{-9}\ \Omega\,\mathrm{cm}^2$ enhance $\rho^{\parallel}$. This is especially obvious by irradiation[3(a)] where isotropy is increasing.

By intercalation of iodine between the BiO layers of 2:2:1:2,[40] $\rho^{\perp}$ was reduced to metalliclike conduction with $\rho^{\perp}(100\ \mathrm{K}) \simeq 1\ \Omega\,\mathrm{cm}$, $\rho^{\parallel}$ and α were enhanced whereas T_c was lowered. All these properties are found by overdoping of 2:2:1:2.[18,32] Thus the author concludes that I creates at E_F states in the BiO layer overdoping the CuO_2 planes and causing resonant tunneling between the planes reducing $\rho^{\perp}$.

Cuprates allow the study of intrinsic or WL conduction by de- or oxygenation[26,27,39] or pressure. The intrinsic conduction with the signature $p^{\parallel} \approx 1$ shows with O removal in $YBa_2Cu_3O_{7-\delta}$ from $\delta \simeq 0.05$ to 0.2 an increase[39]

$$\delta\alpha^i \simeq \alpha^i \quad \text{and } \delta\rho_{OL}^i \simeq 70\ \mu\Omega\,\mathrm{cm}\ . \tag{3.8}$$

The factor of 2 increase of α^i is explained in our model by a decrease of the density of states n_s by a factor of 2, whereas $\delta\rho_{OL}^i \simeq 70\ \mu\Omega\,\mathrm{cm}$ is explained by the retraction of the MII (Sec. II B) at WL. For bulk sintered YBCO (Ref. 41) and for epitaxial films (Ref. 42) with $p \geq 2$, $\delta\alpha^i$ by deoxygenation is in agreement with single-crystal results [Eq. (3.7)].[27] But for $\delta\alpha^i = \alpha^i/4$, the WL resistivity is enlarged, e.g., in Ref. 41 by $\delta R_{bn}^{\parallel} \approx 10 R_{bn}^{\parallel}$ and in Ref. 42 for $\delta\alpha_i = \alpha^i/3$ by $\delta R_{bn}^{\parallel} \simeq 2R_{bn}^{\parallel}$. By irradiation in Ref. 3b $\delta\alpha^i \simeq \alpha^i/3$ has been observed with $\delta R_{bn}^{\parallel} \simeq 50 R_{bn}^{\parallel}$. These drastic $\delta R_{bn}^{\parallel}$ increases are in line with the exponential increase of $R_{bn}^{\parallel}$ in deoxygenation.[26]

Oxygenation of YBCO mainly changes n_s via the oxygenation of the chains which creates states at E_F in the chains. In Bi or Tl cuprates, oxygenation causes states in the Bi (Tl) oxide layer at E_F,[18] able to yield resonant tunnel channels and to increase n_s. This new tunnel channel shows up most clearly in the decrease of $\rho^{\perp}$, $p^{\perp}$, and $\Delta^{\perp}$, whereas $j_c^{\perp}$ increases up to 10^4 A/cm^2.[32,33]

In the above summary, I have shown that $\rho(T)$ can be consistently described by percolation[7] and inter- and intragrain-boundary resistances agreeing with results on

weak links and tunnel channels discussed in Ref. 4. In contrast, the interpretation of the grain-boundary resistances by normal conducting layers is unable to explain the degradation in $R_{bn}^{\parallel}$ ($\Omega\,\mathrm{cm}^2$) between 2 and 5 orders of magnitude. It should be mentioned that $\alpha_i^{\parallel} \simeq 0.5$ $\mu\Omega\,\mathrm{cm/K}$ is an average of $\alpha_b^i \approx 2\alpha_a^i$ in twinned YBCO. Mechanical detwinning often enhanced $\rho(0)$ drastically to values above 100 $\mu\Omega$ cm, likely by strain. Similar analysis of $\rho(T)$ of Bi cuprates[32,43] yields $\alpha^i \simeq 0.6$ $\mu\Omega\,\mathrm{cm/K}$ and $R_{bn}^{\parallel} > 10^{-7}$ $\Omega\,\mathrm{cm}^2$ for melt-cast material. For epitaxial films of 2:2:1:2 $R_{bn}^{G} \approx 10^{-8}$ Ω cm for intragrain weak links has been found slightly above YBCO.

D. Josephson critical current of WL

Following Refs. 4 and 6 and Sec. II C the superconducting properties of WL are j_{cJ}, λ_J, H_{c1J}, and Δ_s. Due to the dominant normal leakage current j_{bl} (Fig. 2), $j_{cJ}^{\parallel} \propto \Delta_s$ does not hold. Instead $j_{cJ}^{\parallel} \propto 1/R_{bn}^{\parallel 2}$ holds and the measured, average j_c may be overshadowed by pinning (Fig. 4). The field dependence $j_{cJ}(H)$ or $\lambda_J(H)$ depends on extension w of WL and on "pinning in and at" WL. So the strength j_{cJ}, the temperature, and the field dependence have to be discussed separately.

1. Josephson coupling strength

Secs. II A and III A have shown that $R_{bn}^{\parallel}$, even for the strongest WL, is dominated by resonant tunneling. According to Eq. (2.8), $j_{cJ}^{\parallel} \propto 1/R_{bn}^{\parallel 2}$ holds, being a measure of the Josephson coupling strengths for type C WL of Fig. 6. Optimal values of j_{cJ} and $j_{cJ}R_{bn}$ are observed for $R_{bn}^{\parallel} \simeq 10^{-9}$ $\Omega\,\mathrm{cm}^2$, with $j_{cJ}R_{bn} \leq 10$ mV, and $j_{cJ} \leq 10^7$ A/cm^2. But even for this type C $j_{cJ} \propto 1/R_{bn}^2$ diminishes[26] by four orders of magnitude with deoxygenation showing that WL coupling depends more sensitively on O content than bulk properties j_c or σ.[27] In all cases for the high conductivity direction $j_{cJ}^{\parallel}R_{bn}^{\parallel} \ll \Delta_0$ and $j_{bl} \approx j_{cJ}$ holds. Perpendicularly in contrast, $j_{cJ}^{\perp}R^{\perp} \simeq \Delta_0\pi/2e$ is observed with small leakage current in parallel for Bi cuprates with the highest $\rho^{\perp}$.[32,34] With oxygenation (overdoping) $\rho^{\perp}$ and $\Delta^{\perp}$ degrade[32] and $j_{c\perp}$ increases like Eq. (3.2). The exponent $m \leq 0.5$ fits to tunnel transfer through 2:2:1:2 and PBCO (Ref. 4) indicating that in both cases one actually observes resonant tunneling of Cooper pairs via intermediate plaques. In ordered Bi or Tl-O plane or Cu chain environment extended plaques form supporting superconductivity. The plaques are distributed inhomogeneously as deduced form $a^{\perp} > 30$ nm [Eq. (3.7)]. As indicated by $j^{\perp}{}_c R^{\perp} \simeq \Delta_0$ the leakage current $j_{bl}^{\perp}$ is fairly small, in line with recent tunnel results[34] and with the above "plaque model."

The Josephson penetration depth λ_J and H_{c1J} resulting from 10^5 A/cm^2 and $\lambda_I \simeq 140$ nm is with [Eqs. (2.9) and 2.10)],

$$\lambda_J \geq 1.2\ \mu\mathrm{m} \quad \text{and} \quad H_{c1J} \leq H_{c1}^{\parallel}\lambda_I/\lambda_J \simeq 100\ \mathrm{Oe}\ , \tag{3.9}$$

typical for strong WL.[28] Values[26,28] of j_{cJ} above 10^6 A/cm^2 or even 5×10^7 A/cm^2 are caused by nanoshorts and by pinning,[25] discussed below. In the perpendicular direction cuprates act as a stack of Josephson junctions yielding for[32]

$$j_c^{\perp} \simeq 200\ \mathrm{A/cm}^2\ (10^4/\mathrm{A\,cm}^2), \quad \lambda^{\perp} \simeq 300\ \mu\mathrm{m}\ (30\ \mu\mathrm{m})$$
$$\text{and} \tag{3.10}$$
$$H_{c1}^{\perp} \simeq 200\ \mathrm{Oe}\ (2000\ \mathrm{Oe})\ .$$

The long shielding lengths $\lambda^{\perp} > 10$ μm have severe consequences for current distributions.

2. Temperature dependence $j_{cJ}(T)$

The surface energy gap Δ_s in Eq. (2.7) shows that the temperature dependence of j_{cJ} is dominated by Δ_s, i.e., by a surface T_c^*. Δ_s and T_c^* are smaller than in the bulk as shown, e.g., by Refs. 30 and 31, where in the high $\sigma^{\parallel}$ directions, $T_c \simeq 88$ K are found, but in low σ, i.e., in large R_{bn} directions, $T_c^* \simeq 84$ K holds. Especially at 77 K, such reduced transition temperatures $T_c^* \simeq 84$ K deteriorate $j_c(77\ \mathrm{K})$ results drastically and so in Sec. III D 1 we compared 4.2 K results only. The different WL T_c^* values and different WL Δ_s values cause a change of the current distribution and percolation in going from the normal to the superconducting state. For example, for well-ordered cuprates[32] $\Delta^{\perp} > \Delta_s^{\parallel}$ holds enhancing $j_c^{\perp}/j_c^{\parallel}$ over the normal conducting $\sigma^{\perp}/\sigma^{\parallel}$ value at T_c, especially because of the activated conduction in $\sigma^{\perp}$ (see Secs. III E 3 a and III E 3 b). Below T_c^* the pair weakening can be cast into a proximity-effect model with[4]

$$j_{cJ}(T) \propto (1-T/T_c)^m \text{ with } m \simeq 2, \quad T \gtrsim T_c/4 \tag{3.11}$$

turning to a $j_{cJ}(T) \propto \tanh\Delta_s/2kT$ dependence with $\Delta_s/2kT_c \approx 1-2$ at low temperatures $T \leq T_c/4$. Such dependences are discussed, e.g., in Refs. 4, 11, 23, 26, or 28.

3. Field dependencies of $j_{cJ}(H)$

In Refs. 21, 23, or 28 and Fig. 1 it is shown that type C WL consists of arrays of strong links ($\varnothing \approx 1$ nm) or nanoshorts which seemingly carry $j_{cJ}^0 \geq 10^7$ A/cm^2. Differences between type C WL, e.g., by angle[23,28] are proposed to be related to a different density of such nanoshorts. The WL type A and B show angle mismatch and hence less current carrying nanoshorts. Types D are intrinsically clean and uniform with a small $j^{\perp} \approx 200$ A/cm^2 (2:2:1:2) (Ref. 32) or $j^{\perp} \approx 10^4$ A/cm^2 (YBCO or overdoped 2:2:1:2 with Pb), accordingly.

Irregular type C WL with nanoshorts in distances r_0 much smaller than fluxon distances $\lambda_0 \gg r_0$ simulate uniform weak links. Then by Frauenhofer-type interference, the field dependence $j_{cJ}(H)$ for $H_e \gg H_{c1J}$ [Eqs. (3.9) and (3.10)] follows:

$$j_{cJ}(H_e) \simeq j_{cJ}(H_0)/(1-H_e/H_0) \quad \text{with } H_0 \approx H_{c1J} \tag{3.12}$$

yielding

$$\lambda_J(H_e) \approx \lambda_J(H_0)(1+1/2\ H_e/H_0)\ .$$

Pinning yields strong deviations from this simple H dependence. For example, the $j_{cJ}(H)$ decrease reaches a plateau for $r_0 \approx \lambda_0$ or increases up to j_{cJ}^0 for $r_0 \approx \lambda_0$:[25]

$$j_{cJ}(H \approx 0) < j_c(H_{\text{opt}}) \approx j_{cJ}^0 \approx 10^{+7} \text{ A/cm}^2 ; \quad H_{\text{opt}} = H_{\text{res}} + H_e . \tag{3.13}$$

Here, H_{res} describes frozen-in fluxons dominantly from vortex-antivortex nucleation near T_c. The vortex pairs are especially likely for thin ($t < \lambda$) films or superconducting quantum interference device arrays as described by the Kosterlitz-Thouless transition.[44] H_{res} is especially large in WL because Josephson fluxons are pinned easily and because there exists $j_{c\text{opt}} > j_{cJ}$ ($H_c \approx 0$).[25] Thus the author proposes the following model for the large residual flux density $\propto H_{\text{res}}$ and its material dependence:[44–46] Vortex-antivortex pairs being created by kT ($\approx kT_c$) get separated and pinned in the bulk[44] and especially at WL.[45] In the bulk the large flux mobility yields some annihilation. In WL annihilation is unlikely due to the strong pinning and due to the existence of an optimal $j_{c\text{opt}}$. In thin films the existence of $j_{c\text{opt}}$ prevents rearrangements reducing $j_{cJ}(H)$ because of the energy needed for such a global rearrangement. Thus the corresponding residual field H_{res} can be quite large as observed by fluctuating residual fields $H_{\text{res}} \leq 1$ kOe.[45] This model explains that $H_{\text{res}} \propto$ flux density increases with WL density[46] or for thinner films.[44] At the surface, flux migrates out. So, an external field H has first to penetrate through the flux free surface regime before interaction starts with the pinned vortex antivortices, i.e., annihilation. The nucleation and penetration through the surface regime occurs for $H_e > H_{c1J}$, like in the vortex-antivortex-free case, and then the annihilation progresses accompanied by a $j_{cJ}(H_{\text{res}} + H_e)$ decrease.

The j_{cJ} decrease [Eq. (3.12)] scales with the flux penetration in a contact area A and may yield new plateaus when optimal rearrangements are possible:

a-axis grains with $a_G \approx 0.2$ μm and $2\lambda_I \approx 0.3$ μm have $A \approx a_G 2\lambda_I$ as a contact area yielding a j_{cJ} decrease up to $H \approx \Phi_0 / A \approx 300$ Oe and $H_{\text{sat}} > 1$ T.[30]

Aligned YBCO (Ref. 24) shows a j_{cJ} decrease up to $H \approx \Phi_0 / A \approx 80$ Oe yielding $a_G \approx 1$ μm and $H_{\text{sat}} \simeq 0.5-1$ T.

Epitaxial films show[23] $H_{\text{sat}} \approx 10-20$ T. The saturation levels $H_{\text{sat}} > 10$ T can be explained by the nanoshorts with diameters below about 1 nm showing $j_{cJ}^0 \geq 10^7$ A/cm^2. This proves[30] the 10 nm contact length discussed in Sec. II and sketched in Fig. 1.

The field dependences in Eqs. (3.12) and (3.13) are modified for thin films of thickness $t < \lambda_I, \lambda_J$. Then fields perpendicular to the films are shielded by the small carrier density t/λ^2 only, yielding as the shielding length

$$\lambda_J^{\perp} = \lambda_J^2 / 2t > \lambda_J , \tag{3.14}$$

enhancing $H_{c1J}^{\perp}$ correspondingly. By demagnetization, the penetration into WL is eased, which may be approximated by[47] the enhancement

$$H_e^* \simeq H_e 1.2w/t , \tag{3.15}$$

with w the width (length) of the WL. For example, Eq. (3.15) explains a flux entry rate $\Delta H_e^* \simeq \Phi_0 t / 1.2w^2$ modulating $j_c(H)$ in Eq. (3.12) or rescales the H_{c1G} flux penetration observed below 1 Oe (Ref. 23) to above about 100 Oe—in line with Table II. Fields parallel to the planes yields flux penetration above 100 Oe [Eq. (3.10)] and long shielding length $\lambda^{\perp}$ being often above sample dimension. It is the opinion of the author that this problem is not thoroughly studied yet.

E. Separation of WL effects in the superconducting state

As summarized in Secs. II C and III D, WL show up in a small Josephson critical current density j_{cJ} and large leakage current $j_{bl}^{\parallel} \approx j_{cJ}^{\parallel}$. Consequently WL can be identified best by the leakage current j_{bl} or by the reduction of $j_{cJ}(T,H)$ resulting in an enhanced Josephson penetration depth $\lambda_J^2 \propto 1/j_{cJ}$ reducing the fluxon entering field H_{c1J}. The direct identification of j_{cJ} is possible only if j_{cJ} is the weakest part in the conduction path. This has been achieved by constrictions with natural or artificial WL.[23,26,28]

1. *Surface impendance*

The surface resistance is dominated by the normal leakage current $j_{bl} \propto 1/R_{bl}$ of WL as summarized by the author in Eq. (2.11).[11] $j_{bl} \simeq j_{bn} - j_{cJ}$, R_J, and λ_J depend on T slowly only via j_{cJ} (Eq. 3.11) yielding, e.g.,

$$j_{bl} \simeq j_{bl}(0)(1+ct) (c \approx 1, t = T/T_c < 0.5) .$$

Aside of the leakage current $j_{bl} \propto 1/R_{bl}$, the surface resistance yields a sensitive measure of λ_J and H_{c1J} as discussed in Refs. 11 and 48 in detail. Equation (2.11) allows an unique identification of R_{bl}, λ_J, and H_{c1J} of inter- and intragrain WL—see Table II.

This rf identification is a proper average, not masked by "best current path effects" dominating in dc. The enhancement of the penetration depth by percolation [Eq. (2.5)] and $\lambda_J > \lambda_I$ is discussed for 2:2:1:2 in Ref. 43 and in general in Ref. 11: λ_J and grows with a field like H^2 changing over to a linear increase at H_{c1J}.

2. *j_{cJ} of intergrain WL*

The small value of $j_{cJ} \leq 10^2$ A/cm^2 and the strong degradation of j_{cJ} with H between 0.5 and 100 Oe (Table II and Fig. 4) yields an easy separation of $j_{cJ}(T,H)$ from j_c.[24] Such intergrain WL have a large Josephson penetration depth $\lambda_J \geq 10$ μm and $j_{bl} \simeq j_{bn}$ and thus yield large surface resistances being a function of T, H, and ω according to Eq. (2.11) as discussed in Refs. 11 and 48.

3. *j_{cG} of intragrain WL*

The large critical currents of WL $j_{cG} \geq 10^4$ A/cm^2 and by pinning[28] $j_{cp} \geq 10^4$ A/cm^2 make a direct identification of $j_{cG}(T,H)$ difficult by critical current measurements. Constrictions (Refs. 14, 23, 26, 28, and 37) containing one

WL show j_{cG} between 10^4 and above 10^7 A/cm^2. The field dependences[23–25] are in line with nanoshorts (Fig. 1) making up WL. But the identification of WL $j_{cG}(T,H)$ in extended material is still controversial.[37] To make the situation worth, bulk flux pinning adjacent to WL degrades $j_{cG}(T,H)$ weakly only, see Ref. 49. In this connection the basic $j_{cJ}(H)$ degradation mechanism has to be restated. The dephasing of both WL banks by flux penetration into WL degrades $j_{cJ}(H)$ as, e.g., discussed in Ref. 24. This process is easily envisioned in epitaxial films[23,30,31] but in bulk material multiconnectivity may forbid dephasing and flux penetration into WL. In grain-aligned material this hindering of dephasing is enforced not only by alignment yielding a higher density of nanoshorts[24] but also by the brick-wall-type conduction path $j_c^{\perp}$ discussed below.[50] Then bulk pinning defines the dc transport current and intragrain WL can be identified only by the leakage current, i.e., the surface resistance discussed in Sec. III E1.

In epitaxial films the $j_c(H)$ measurements and morphology yields the following results. In c-axis films[9] $a \simeq 1$ μm and $2\lambda_I \simeq 0.3$ μm yield $\Phi_0/A \simeq 70$ Oe as saturation field. Then j_{cJ}(opt) is reached[25] and bulk pinning dominates at higher fields, in line with experiments.[26,28] In the a-axis films of Ref. 30, $a \simeq 0.2$ μm holds being smaller than $2\lambda_l$. Hence no simple dephasing of "one WL" is possible and above $\Phi_0/A \simeq 350$ Oe dominates bulk pinning.

a. j_c and j_{cG} in grain-aligned YBCO. Grain-aligned or "single-crystalline" YBCO show $j_c(T,H)$ dependences not allowing an unique identification of WL and their $j_{cJ}(T,H)$. This is despite the fact that STM (Ref. 9) in Fig. 5 shows clearly islands and intragrain WL. By deoxygenation, magnetization results are indicative for a granularity and WL in $j_c(T,H)$.[51,52] Deoxygenation reduces j_{cJ} drastically according to Eq. (3.1), hence granularity occurs via $j_{cJ} < j_{cp}$, especially close to T_c. The results[51,52] are a strong indication for the above WL model. The anisotropy of j_c in grain-aligned material $j_c^{\perp}/j_c^{\parallel} \leq 0.05$ for $\alpha^{\perp}/\alpha^{\parallel} \simeq 80$ with $j_c^{\parallel}$ (77 K) $\simeq 7 \times 10^4$ A/cm^2 and $\alpha^{\parallel} \simeq 1.3$ $\mu\Omega$ cm/K seems to be governed by WL also.[53] Remarkably, there is the reduction of the anisotropy from 100 above T_c to about 20 below T_c with $j_c^{\perp} \approx 10^3$ A/cm^2. This proves that the perpendicular superconducting channel is stronger relatively than the corresponding normal conducting channel, even for the low value of $j_c^{\perp} \approx 10^3$ A/cm^2. This $j_c^{\perp}$ is smaller than the intrinsic $j_c^{\perp}$ [Eq. (2.4)] proving the strong degradation of c-axis surfaces of YBCO (Ref. 17) in the melt-textured growth process,[53] discussed in Sec. III D.

b. j_c and j_{cG} in grain-aligned Bi cuprates. In melt-cast, i.e., grain-aligned Bi cuprates, high values

$$j_c(T < 30 \text{ K}, H \approx 10 \text{ T}) \approx 10^5 \text{ A/cm}^2$$

have been found.[37] In dc and rf measurements this material shows WL-like[43] sintered YBCO,[11] discussed above. So the $j_c(T,H)$ superiority of 2:2:1:2 or 2:2:2:3 materials is not obvious. But YBCO shows usually degraded c-axis surfaces,[17] in contrast to Bi cuprates. So the brick-wall[50] current path $j_c^{\perp}$ is degraded in Y cuprates, in contrast to Bi cuprates. The strong c-axis current $j_c^{\perp} \leq 10^4$ A/cm^2 by the brick-wall-type morphology of Bi-Sr-Ca-Cu-O (BSCCO) hinders fluxons to penetrate into WL and hence the dephasing of both banks. Under these circumstances bulk pinning defines the transport current. The observation[54] of low-T_c material at WL in melt-cast Bi cuprates does not change the above analysis. First, $R_{bn} \geq 10^{-7}$ Ω cm^2 proves[43] the dominance of an insulating seam at WL. Second, a normal conductor in addition to an insulator reduces H_{c1J} further and yields field dependencies at rather low fields, as has been observed in rf measurements.[43]

IV. SUMMARY

In the above analysis ample evidence for WL is presented by normal and superconducting measurements. Combining $\rho(T)$ and morphology measurements, WL boundary resistances $R_{bn}^{\parallel} \simeq 10^{-7}$–$10^{-9}$ Ω cm^2 are deduced. In the superconducting state the corresponding WL Josephson critical currents are $j_{cJ} \simeq 10^2$–10^7 A/cm^2. Such R_{bn} and j_{cJ} values are explained by an insulating seam containing localized states allowing resonant tunneling. dc measures the best current paths and thus some WL may be circumvented. In contrast, rf currents average properly yielding j_{cJ} and j_{bl}. Defects enhance $\sigma^{\perp}$ and $j_c^{\perp}$ and, especially as weak links, reduce $\sigma^{\parallel}$ and $j_c^{\parallel}$. In contrast to YBCO, for Bi cuprates the intergranular $\sigma^{\perp}$ and $j_c^{\perp}$ stay large being the surface physics foundation of the brick-wall model.

ACKNOWLEDGMENTS

The author acknowledges clarifying discussions with S. Babcock, I. Bozovic, A. Braginski, B. Buhrman, P. Chaudhari, Ch. B. Eom, G. Godel, M. Hawley, R. Kleiner, H. Küpfer, H. Lang, and D. Larbalestier.

[1] W. E. Pickett, H. H. Krakauer, R. E. Cohen, and D. J. Single, Science **255**, 46 (1992).

[2] See, e.g., L. H. Greene and B. G. Bagley, in *Physical Properties of High-Temperature Superconductors II,* edited by D. M. Ginsberg (World Scientific, Singapore, 1991), p. 509.

[3] (a) M. V. Sadovskii, in *Proceedings of the International Workshop on the Effect of Strong Disordering in HiTc-SC, Zarechny, June 1990* (U.S.S.R. Academy of Sciences, Moscow, 1990), p. 32. (b) J. M. Valles, A. E. White, K. T. Short, R. C. Dynes, J. P. Gerno, A. F. J. Levi, M. Anzlawer, and K. Baldwin, Phys. Rev. B **39**, 11 599 (1989). (c) C. Quitmann, D. Andrich, C. Jarchow, M. Fleuster, B. Beschoten, G. Güntherodt, V. V. Moshchalkov, G. Mante, and R. Manzke, Phys. Rev. B **46**, 11 813 (1992).

[4] J. Halbritter, Phys. Rev. B **46**, 14 861 (1992).

[5] S. E. Babcock and D. C. Larbalestier, J. Mater. Res. **5**, 919 (1990); S. Babcock, MRS Bull. 20 (August 1992).

[6] J. Halbritter, J. Superconduct. **5**, 171 (1992); **5**, 333 (1992).

[7] J. Halbritter, Int. J. Mod. Phys. B **3**, 719 (1989); and in *Superconductivity and Applications,* edited by H. S. Kwok (Plenum, New York, 1990), p. 351.

[8] J. C. Phillips, Phys. Rev. B **46**, 8542 (1992).

[9]H. P. Lang, T. Frey, and H. J. Güntherodt, Europhys. Lett. **15**, 667 (1991); M. E. Hawley *et al.*, Ultramicroscopy **42-44**, 705 (1992), and other STM papers in this volume.

[10]See, e.g., M. Tinkham and C. J. Lobb, *Solid State Physics: Advances in Research and Applications,* edited by H. Ehrenreich and D. Turnbull (Academic, New York, 1989), Vol. 42, p. 91.

[11]J. Halbritter, J. Appl. Phys. **68**, 6315 (1990); **71**, 339 (1992).

[12]T. L. Barr and C. R. Brundle, Phys. Rev. B **46**, 9199 (1992).

[13]See, e.g., S. T. Chui and J. D. Weeks, Phys. Rev. B **14**, 4978 (1976).

[14]B. H. Moeckly, D. K. Lathrop, and R. A. Buhrman, Phys. Rev. B **47**, 400 (1993).

[15]H. L. Edwards, J. T. Markert, and A. L. de Lozanne, Phys. Rev. Lett. **69**, 2967 (1992); H. Behner, K. Rührnschopf, G. Wedler, and W. Rauch, Physica C **208**, 419 (1983).

[16]J. Halbritter, P. Walk, H.-J. Mathes, B. Häuser, and H. Rogalla, Z. Phys. B **73**, 277 (1988); *High-T_c Superconducting Thin Films, Devices, and Applications,* Proceedings of the 1988 Topical Conference on High-T_c Superconducting Thin Films, Devices, and Applications of the AVS, Atlanta, Ga., edited by Giorgio Margaritordo, Robert Joynt, and Marshall Onellion, AIP Conf. Proc. No. 182 (AIP, New York, 1989), p. 208.

[17]A. M. Aarnink, Ph.D. thesis, University of Twente, Enschede, 1992; A. M. Aarnink, J. Gao, H. Rogalla, and A. van Silfhout, Appl. Surf. Sci. **55**, 117 (1992); H. Behner, K. Rührnschopf, W. Rauch, and G. Wedler, Appl. Surf. Sci. **68**, 179 (1993).

[18]B. O. Wells, Z. X. Shen, D. S. Dessau, W. E. Spicer, C. G. Olson, D. B. Mitzi, A. Kapitulnik, R. S. List, and A. Arko, Phys. Rev. Lett. **65**, 3056 (1990).

[19]A. G. M. Jansen, A. P. van Gelder, and P. Wyder, J. Phys. C **13**, 6073 (1980).

[20]J. Halbritter, Surf. Sci. **122**, 80 (1982); **153**, 80 (1982); J. Appl. Phys. **58**, 1320 (1985).

[21]S. Babcock (unpublished).

[22]U. Poppe, N. Klein, K. Dähne, H. Soltner, C. L. Jia, B. Kabius, K. Urban, A. Lubig, K. Schmidt, S. Hensen, S. Orbach, G. Müller, and H. Piel, J. Appl. Phys. **71**, 5572 (1992).

[23]E. Sarnelli, P. Chaudhari, M. Däumling, and J. A. Lacey, IEEE Trans. Appl. Superconduct. **3**, 2329 (1993).

[24]J. W. Ekin *et al.*, Physica C **160**, 489 (1989); J. Appl. Phys. **68**, 2285 (1990).

[25]R. Fehrenbacher, V. B. Geshkenbein, and G. Blatter, Phys. Rev. B **45**, 5450 (1992).

[26]S. E. Russek, Ph.D. thesis, Cornell University, 1990; S. E. Russek, D. K. Lathrop, B. H. Moeckly, R. A. Buhrman, D. H. Shin, and J. Silcox, Appl. Phys. Lett. **57**, 1155 (1990).

[27]H. Claus, M. Braun, A. Erb, K. Röhberg, B. Runtsch, H. Wühl, G. Bräuchle, P. Schweib, G. Müller-Vogt, and H. v. Löhneysen, Physica C **198**, 42 (1992).

[28]D. Dimos, P. Chaudhari, and J. Mannhart, Phys. Rev. B **41**, 4038 (1990); R. Gross, P. Chaudhari, M. Kawasaki, and A. Gupta, Phys. Rev. B **42**, 10 735 (1990).

[29]Y. Zhang, M. Mück, M. Bode, K. Herrmann, J. Schubert, W. Zander, A. Braginski, and C. Heiden, Appl. Phys. Lett. **60**, 2303 (1992).

[30]C. B. Eom, A. F. Marshall, Y. Suzuki, B. Boyer, R. F. W. Plase, T. H. Geballe, R. B. van Dover, and J. M. Phillips, Phys. Rev. B **46**, 11 902 (1992).

[31]W. A. M. Aarnink, E. M. C. M. Reuvekamp, M. A. J. Verhoeven, M. V. Pedyash, G. J. Gerritsma, A. van Silfhout, and H. Rogalla, Appl. Phys. Lett. **61**, 607 (1992).

[32]R. Kleiner, Ph.D. thesis, TU, Munich, 1992; and (private communication).

[33]S. L. Cooper, P. Nyhns, D. Raznik, M. V. Klein, W. C. Lee, D. M. Ginsberg, B. W. Veal, A. P. Paulikas, and B. Dabrowski, Phys. Rev. Lett. **70**, 1533 (1993).

[34]I. Bozovic and J. Eckstein (unpublished); B. A. Aminov *et al.*, J. Alloys Compounds **195**, 551 (1993); T. Hasegawa *et al.*, J. Phys. Chem. Solids **53**, 1645 (1992).

[35]M. Lee, D. Lew, C. B. Eom, T. H. Geballe, M. R. Beasley, Appl. Phys. Lett. **57**, 1152 (1990); Mark Lee, Ph.D. thesis, Stanford University, 1990.

[36]R. Hahn, T. Schäffter, J. Klockau, and G. Fotheringham, IEEE Trans. Appl. Superconduct. **3**, 2379 (1993); Jack Eckin and Steven Russek (unpublished); R. P. Robertazzi, A. W. Kleinsasser, R. B. Laibowitz, R. H. Koch, and K. G. Stawiasz, Phys. Rev. B **46**, 8456 (1992).

[37]D. C. Larbalestier *et al.*, Phys. Today **44**(6), 74 (1991).

[38]G. Weigang and K. Winzer, Z. Phys. B **77**, 11 (1989); K. Winzer and G. Kumm, *ibid.*, **83**, 317 (1991); K. Winzer, G. Kumm, P. Maass, H. Thomas, E. Schwarzmann, A. Aghaie, and F. Ladenberger, Ann. Phys. (Leipzig) **1**, 479 (1992).

[39]L. Forro, V. Ilakovac, J. R. Cooper, C. Ayache, and J.-Y. Henry, Phys. Rev. B **46**, 6626 (1992).

[40]X. D. Xiang, W. A. Vareka, A. Zettl, J. L. Corkill, M. L. Cohen, N. Kijima, and R. Gronsky, Phys. Rev. Lett. **68**, 530 (1993).

[41]J. R. Cooper, S. D. Obertelli, A. Carrington, and J. W. Loran, Phys. Rev. B **44**, 12 086 (1991).

[42]R. Feenstra, D. K. Christen, C. E. Klabunde, and J. D. Budai, Phys. Rev. B **45**, 7555 (1992).

[43]G. Godel, N. Gold, J. Hasse, J. Halbritter, and J. Bock (unpublished).

[44]See, e.g., C. T. Rogers, K. E. Myers, J. U. Eckstein, and I. Bozovic, Phys. Rev. Lett. **69**, 160 (1992).

[45]T. Tamegai, L. Krusin-Elbaum, P. Santhanam, M. J. Brady, W. T. Masselink, C. Feild, and F. Holtzberg, Phys. Rev. B **45**, 2589 (1992).

[46]A. F. Hebard, A. T. Fiory, M. P. Siegal, J. M. Phillips, and R. C. Haddon, Phys. Rev. B **44**, 9753 (1991).

[47]P. A. Rosenthal, M. R. Beasley, K. Char, M. S. Collough, and G. Zaharchuk, Appl. Phys. Lett. **59**, 3482 (1991).

[48]J. Wosik, L. M. Xie, J. Halbritter, R. Chan, A. Samaan, J. C. Wolfe, V. Selvamanicham, and K. Salama, IEEE Trans. Appl. Superconduct. **3**, 1432 (1993); J. Halbritter, J. Alloys Compounds **195**, 579 (1993).

[49]M. V. Fistul, Pis'ma Zh. Eksp. Teor. Fiz. **49**, 95 (1989) [JETP Lett. **49**, 113 (1989)].

[50]See, e.g., N. Adamopoulos and J. E. Evetts, IEEE Trans. Appl. Superconduct. **3**, 1257 (1993); L. Bulaevskii, J. R. Clem, L. I. Glazman, and A. P. Malozemoff, Phys. Rev. B **45**, 2545 (1992).

[51]M. Däumling, J. M. Seuntjens, and D. C. Larbalestier, Nature (London) **346**, 332 (1990).

[52]M. S. Osofsky, J. L. Cohn, E. F. Shelton, M. M. Miller, R. J. Soulen, S. A. Wolf, and T. A. Vanderah, Phys. Rev. B **45**, 4916 (1992).

[53]V. Selvamanickam and K. Salama, Appl. Phys. Lett. **57**, 1575 (1990).

[54]A. Umezawa, Y. Feng, H. S. Edelman, Y. E. High, D. C. Larbalestier, Y. S. Sung, E. E. Hellstrom, and S. Flesher, Physica C **198**, 261 (1992).

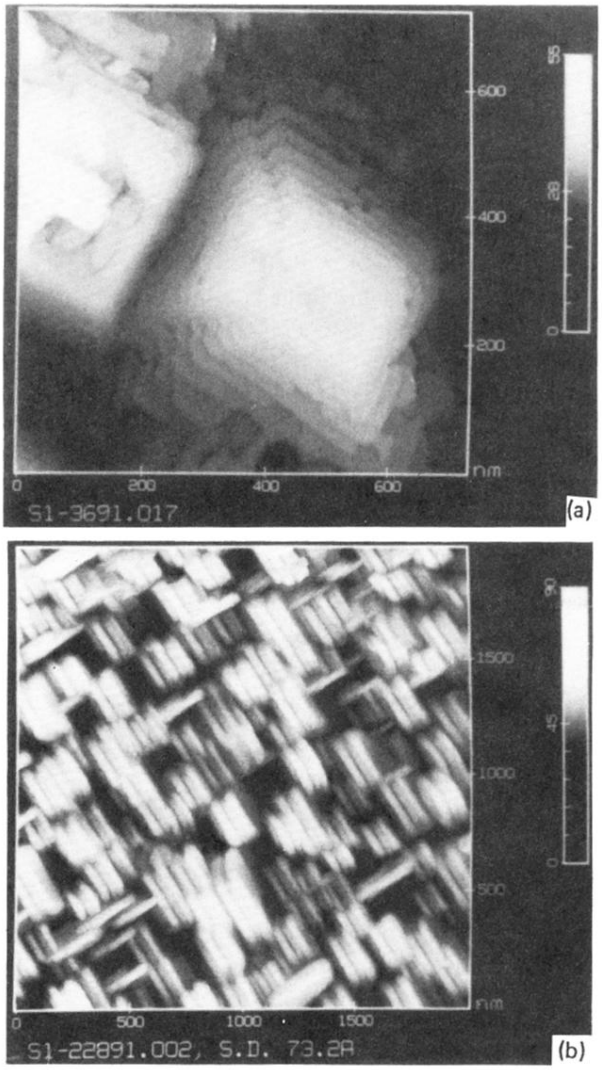

FIG. 5. Typical STM image of $YBa_2Cu_3O_7$ 200-nm thick deposited on MgO (100) single-crystal substrates at standard deposition conditions. (a) *c*-axis films with grains of about 0.5–1 μm. (b) *a*-axis films with grains of about 0.2 μm length (Hawley *et al.*, Ref. 9).